Observation of a strange nonchaotic attractor in a multistable potential

Ting Zhou and Frank Moss
Department of Physics, University of Missouri at St. Louis, St. Louis, Missouri 63121

Adi Bulsara
NCCOSC-RDT and E Division, Materials Research Branch, San Diego, California 92152

(Received 16 September 1991)

Attractors which are not chaotic but nevertheless display "strange" geometric properties have been the subject of a number of studies since they were studied in certain quasiperiodically forced maps, by Grebogi *et al.* [Physica **13D**, 26 (1984)]. The attractors, as defined by these authors, are *nonchaotic,* since they are characterized by Lyapunov exponents which are smaller than zero; but are, however, *strange* since they display geometric properties unlike either limit cycles or quasiperiodic attractors. The attractors are produced by dissipative, nonlinear systems which are driven by two periodic external forces whose frequencies are incommensurate. Strange nonchaotic attractors have been observed in numerical experiments with a variety of bistable and monostable nonlinear oscillators as well as in one ingenious experiment, designed by Ditto *et al.* [Phys. Rev. Lett. **65**, 533 (1990)], using a forced, free standing beam whose mechanical properties could be externally controlled by magnetic fields. We study here a nonlinear oscillator with a multistable potential both numerically and with an analog simulator. The dynamics mimics that of the internal magnetic flux through an underdamped, multistable, superconducting quantum interference device which is quasiperiodically forced. We report measurements and numerical computations of the power spectra, invariant density, and Poincaré sections. Precision numerical computations were used to study the Lyapunov exponents and to observe the destruction of a chaotic attractor and its replacement by a strange nonchaotic one.

PACS number(s): 05.45.+b, 74.40.+k

I. INTRODUCTION

Recently there has been much interest in the properties of quasiperiodically driven nonlinear oscillators of various types. In addition to the more well known dynamical behaviors which result in two-frequency quasiperiodic, three-frequency quasiperiodic, and chaotic attractors, such oscillators have been shown to exhibit a new type of dynamical behavior leading to what are termed *strange, nonchaotic attractors* (SNCA's). This behavior was demonstrated analytically and shown to be structurally stable [1], and subsequently verified in numerical iterations of maps, representing dissipative nonlinear systems with periodic or bistable potentials, driven by two periodic forces with incommensurate frequencies, that is, quasiperiodic forcing [1–6]. Moreover, a SNCA has been observed also in the map representation of an infinitely damped system [2,3] which shows no chaos or three-frequency quasiperiodicity. Though some early doubts existed [2], the SNCA's observed in these systems were later shown to exist on a subset of parameter space of measure greater than zero [2–5]. Since the SNCA's were numerically demonstrated in the resistively shunted Josephson model [2–4] and in an oscillator with the standard quartic potential (Duffing oscillator), which serves as a generic representation of a variety of realizable bistable nonlinear systems, and since they exist on a positive-measure subset of parameter space, it seemed reasonable that they could be discovered in an actual experiment. Indeed, the experimental demonstration of the existence of a SNCA in a quasiperiodically forced, free-standing beam of magnetic material whose mechanical properties can be externally controlled has been recently accomplished [7,8]. In addition, extensive numerical studies on a model of the magnetic beam apparatus based on the parametrically driven Duffing oscillator have been carried out [8].

The emphasis of much of the numerical work has been on the development of criteria by which SNCA's could unambiguously be characterized and on studies of the route to chaos in two-frequency quasiperiodically forced systems. SNCA's show a largest Lyapunov exponent which is nonpositive, hence the term *nonchaotic.* Beyond that, the two most useful characterizations which have emerged are based on the power spectrum and on the information dimension D_1 extracted from a Poincaré section. The Poincaré section itself also displays differences from those of chaotic, quasiperiodic, or periodic attractors: in theory, its structure is everywhere single valued but everywhere discontinuous, hence the term *strange.* In a typical system, for example, the quasiperiodically driven pendulum, the two Lyapunov exponents (of the reduced map, created by sampling the two variables in phase with one of the driving functions) are found to be zero and smaller than zero, respectively [4]. Following the Kaplan-Yorke conjucture [9], the information dimension of such an attractor should therefore be unity [6]. The one experiment which has been accomplished [7] measured a somewhat larger value $D_1 \cong 1.3$. The numerical experiments of Ding, Grebogi, and Ott [6] yielded

values of $D_1 \cong 1.2$ for the reduced map of the pendulum and $D_1 \cong 0.9$ for a quasiperiodically forced circle map. We show here in Sec. III that careful measurements ($\cong 100\,000$ points in the Poincaré section) on an analog simulator result in a value in quite good agreement with these, $D_1 \cong 1.2$, which can be compared to our value of $D_1 \cong 1.6$ in a very close region of parameter space which is chaotic. The following additional characterization has been developed. From the power spectrum, the number of peaks $N(\sigma)$ exceeding a threshold amplitude σ obeys a simple power-law scaling unlike those for two-frequency quasiperiodicity or for chaos [2,3]. Specifically,

$$N(\sigma) \propto \sigma^{-\alpha} \text{ with } 1 < \alpha < 2 \tag{1a}$$

for the SNCA,

$$N(\sigma) \propto \ln\left[\frac{1}{\sigma}\right] \tag{1b}$$

for two-frequency quasiperiodicity, and

$$N(\sigma) \propto \left[\ln\left[\frac{1}{\sigma}\right]\right]^2 \tag{1c}$$

for three-frequency quasiperiodicity. All of these characterizations have now been investigated numerically in the actual experiment and in the analog simulation described here. Some of them have been used in numerical studies on SNCA's in the Van der Pol and other oscillators [10–13]. Studies of the quasiperiodically forced Duffing oscillator were accomplished by Wiggins [14] and, in an interesting experiment with a mechanical oscillator which can be represented by the generic Duffing system [14], by Moon and Holmes [15]. In neither Ref. [14] nor Ref. [15], however, was strange nonchaotic dynamics reported.

In this paper, we investigate the existence of SNCA's and the transition to chaos both by digital numerical simulation and by measurements made on an analog simulator of a version of the pendulum equation which has been used to represent the radio-frequency-driven superconducting quantum interference device (SQUID) with inertia and finite damping:

$$\ddot{x} + k\dot{x} = -\frac{dU(x)}{dx} + q_1 \sin\omega_1 t + q_2 \sin\omega_2 t \ , \tag{2}$$

where the ratio of the two frequencies is the golden mean

$$\frac{\omega_1}{\omega_2} = \frac{1+\sqrt{5}}{2} \ . \tag{3}$$

The potential used in this work was

$$U(x) = \frac{x^2}{2} - \left[\frac{\beta}{2\pi}\right] \cos 2\pi x \ , \tag{4}$$

and for all the results reported here we took $\beta = 2$, which results in the tristable potential shown in Fig. 1. This contrasts with the single previous experiments [7,8] which used a more or less symmetric bistable potential, and all of the previous numerical work which used either periodic or bistable potentials. Our motivation for this work was to demonstrate the existence of SNCA's in this particular potential by experimental measurements on a real physical system, the analog simulator, and thereby to demonstrate the practicality of an experiment on a system with a similar potential, perhaps a *r.f* SQUID. Our results further illustrate the robust properties of this dynamics and the ease with which it can be observed in real physical systems.

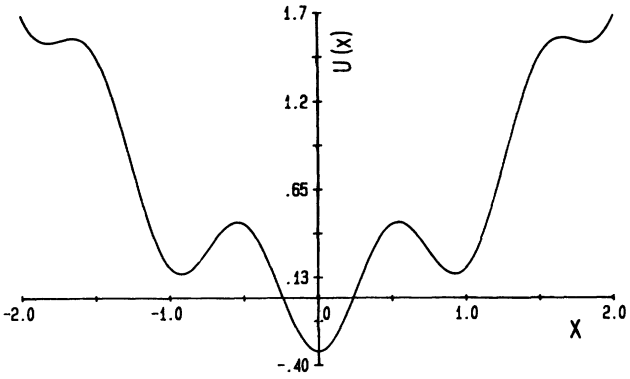

FIG. 1. A plot of Eq. (4) with $\beta = 2$, which was the potential used in this work.

In Sec. II, we describe the simulator together with associated apparatus and the method of obtaining experimental data from it. The results from the analog simulator are backed up by numerical experiments, the methods for which are also described in this section. In Sec. III, we display characteristic results, in particular those for the information dimension, Lyapunov exponent, and invariant density for both chaotic and strange nonchaotic attractors. Measurements of representative power spectra are displayed and analyzed according to Eqs. (1). Moreover, we demonstrate that a SNCA can destroy and replace a chaotic attractor under the action of a single control parameter. We display this result in the style of a phase transition, using the Lyapunov exponent as the order parameter. In Sec. IV, we summarize our results and suggest future experiments.

II. SIMULATION TECHNIQUES

Analog simulators for various applications have been described before [15] in both antique [16] and modern [17] versions. Our simulator of the dynamics of Eqs. (2) and (4) is shown in Fig. 2. It operates over a dynamic range of ± 10 V with a resolution (nearly an order of magnitude above the inherent circuit noise) of $\cong$ 10 mV. The voltages $x(t)$ and $\dot{x}(t)$ were digitized in pairs at 12-bit resolution by a Data Translation Model DT2828 analog-to-digital converter (ADC), which had a throughput of 130 kHz, and input to a Model AT personal computer (PC-AT). The PC was then used to compute and suitably average the power spectrum of $x(t)$ or the Poincaré map of x and $\dot{x}$. For the Poincaré map, the ADC was triggered by a pulse from the higher-frequency one of two Comstron frequency synthesizers. The power spectra were obtained from free-running time series, i.e., time series which were obtained without the trigger pulse from

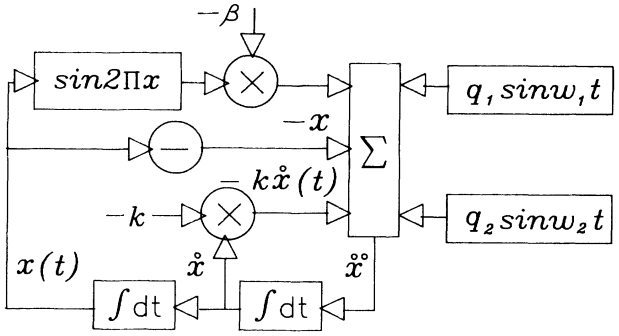

$$\ddot{x}^{\circ} = -k\dot{x} - x - \beta \sin 2\Pi x + q_1 \sin w_1 t + q_2 \sin w_2 t$$

FIG. 2. Schematic diagram of the analog simulator. The circles marked (×) are analog devices AD534 voltage-multiplier chips; the sine chip is an AD639; the integrators are operational amplifiers with feedback capacitors; and summation is accomplished by an operational amplifier with multiple input resistors. The approximately irrational forcing is accomplished with two Comstron frequency synthesizers operated at $f_1 = 3.5810$ kHz and $f_2 = 2.2131$ kHz which have a resolution of 0.1 Hz and a short-term stability of a few parts in 10^9. The time constant of the integrators was 10^{-4} s. The voltages $x(t)$ and $\dot{x}(t)$ were sampled and digitized in pairs upon arrival of a transistor-transistor-logic trigger pulse from the higher-frequency synthesizer.

the synthesizer.

It is important that the simulator be driven by signal generators of higher resolution and better frequency stability than is normally obtainable from ordinary equipment. Frequency synthesizers are therefore necessary in order that relative frequency drift not wash out the special dynamical effects being sought. Even so, the ratio of the synthesized frequencies could only approximate the number shown in Eq. (3) to the fourth decimal place. As shown below, by the agreement of our measurements with digital numerical simulations, this precision was evidently sufficient. The simulator was operated with a voltage-scale factor of unity, which meant that voltage measurements taken from it were numerically equivalent to digital solutions of Eq. (2). The simulator does, however, scale time by a factor equal to the integrator time constant τ_i, so that for the digital simulations, the frequencies must be interpreted as dimensionless quantities $\omega' = \omega\tau_i$. Since the integrator time constant was always 10^{-4} s, the dimensionless frequencies for use in the digital simulations of Eq. (2) were $\omega'_{1,2} = 2.2500$ and 1.3905 ± 0.0001, respectively. It is also to be noted that the stability of a few parts in 10^9 is much greater than the fourth-decimal-place precision achieved.

The steady-state accuracy of the analog simulator was estimated to be approximately 1%, and was determined by the precision of the resistors used. The accuracy of the AD534L chip is 0.25%. The time scaling accuracy of $\cong$ 5% was determined by the precision of the feedback capacitors in the integrators. Our simulator was operated in a bandwidth of 20 kHz, but the largest frequency in our data never exceeded 5 kHz. In order to take advantage of the "small-signal" linearity of our operational amplifiers, the simulator was operated over an output range of $\pm$ 2 V instead of the maximum usable range of $\pm$ 10 V. In effect, the dynamics sampled frequently only the two potential wells at $\cong \pm$ 0.9 V, as shown in Fig. 1, and only much less frequently visited the higher-order local minima. A Poincaré map of 10 000 pairs of points could be obtained in a few seconds. Speed is one advantage of analog simulation.

The digital simulations were accomplished using standard techniques. Specifically, the method used to calculate the Lyapunov spectrum is that due to Shimada and Nagashima and Benettin *et al.* [18]. The actual computer code used was that due to Wolf *et al.* [19] with some modifications. The Lyapunov exponent was computed from trajectories and averaged until convergence to less than 10^{-4} was achieved. For the $q_2 = 0.38$ (chaotic) attractor 3731 trajectories were required for convergence, while the $q_2 = 0.88$ (strange nonchaotic) attractor required 7000. The information dimension was obtained from the complete three-dimensional phase space using typically 30 000 trajectories. These numerical determinations of D_I were in good agreement with those obtained from the two-dimensional Poincaré sections in the analog simulations with $D_I^{3d} - 1 = D_I^{2d}$.

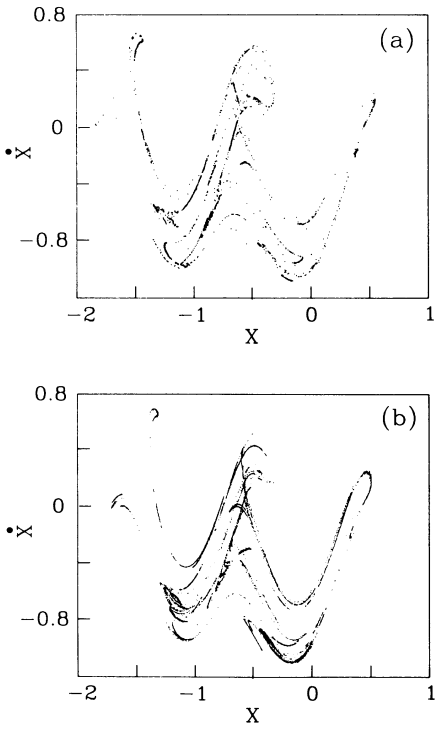

FIG. 3. A SNCA for $k = \beta = 2$ and $q_1 = 2.768$, which are henceforth identified as the "fixed conditions" and with control parameter $q_2 = 0.88$, from the dynamics of Eqs. (2)–(4). (a) Measured on the analog simulator with 10 000 points displayed, and (b) obtained by digital simulation for the same conditions with 30 000 points displayed. The Lyapunov exponent, obtained as described in the text, was $\lambda = -0.150$ for this attractor.

A typical Poincaré map of a SNCA for this system is shown in Fig. 3. The attractor measured with the analog simulator is shown in Fig. 3(a) and can be compared to one obtained for the same conditions by digital simulation shown in Fig. 3(b). The attractors are quite similar, though the digital simulation has fewer points, and the fine scale of the analog attractor is somewhat obscured by noise. Nevertheless, the agreement is quite convincing. Below, we discuss these and additional data in more detail.

III. RESULTS

Figure 3 shows a SNCA measured for $q_2=0.88$ and other conditions fixed as indicated in the figure caption. Throughout, we regard q_2 as a control parameter. We show, in Fig. 4, a chaotic attractor, again obtained from analog (a) and digital (b) simulations. This attractor was obtained for $q_2=0.38$, and the digitally obtained Lyapunov exponent was $\lambda=0.156$. At this point, the only criterion which we have used for identifying the attractor type, apart from the obvious difference in appearance (with the attractor in Fig. 3 appearing more like the description [1,3] "everywhere discontinuous but single valued") is the sign of the Lyapunov exponent. We shall now apply the other criteria outlined in Sec. I.

Two power spectra, measured on the analog simulator for the fixed conditions, are shown in Fig. 5(a) with $q_2=0.88$ and Fig. 6(a) with $q_2=0.38$, that is, for condi-

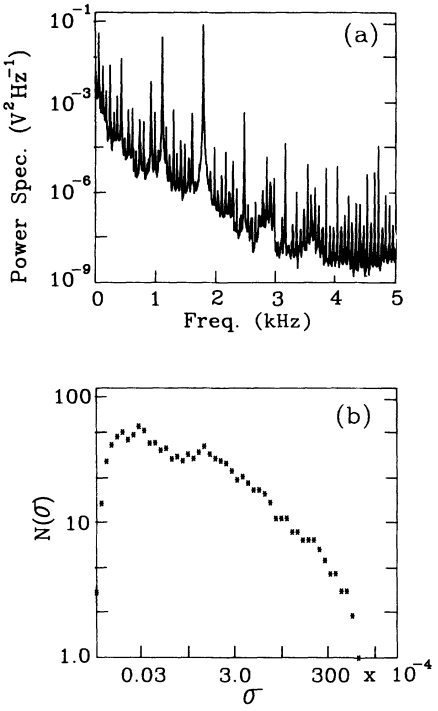

FIG. 5. (a) A power spectrum obtained from the analog simulator for the fixed conditions and $q_2=0.88$ (SNCA), and (b) the threshold dependence of the number of peaks $N(\sigma)$ with amplitudes greater than the threshold σ.

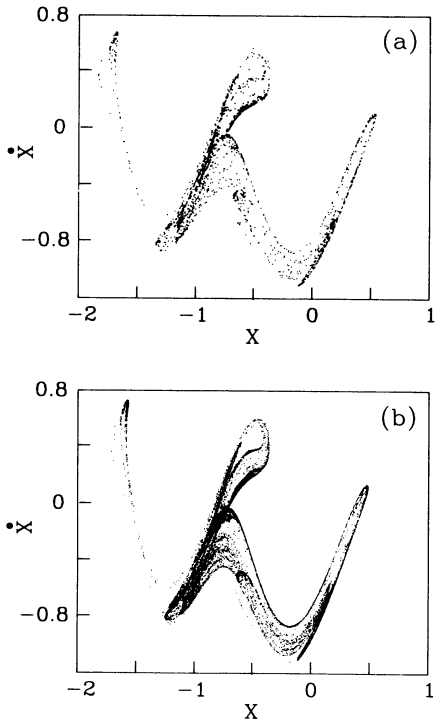

FIG. 4. A chaotic attractor for the fixed conditions with $q_2=0.38$. (a) Measured on the analog simulator (10^4 points), and (b) by digital simulation (3×10^4 points) from which $\lambda=0.156$ was obtained.

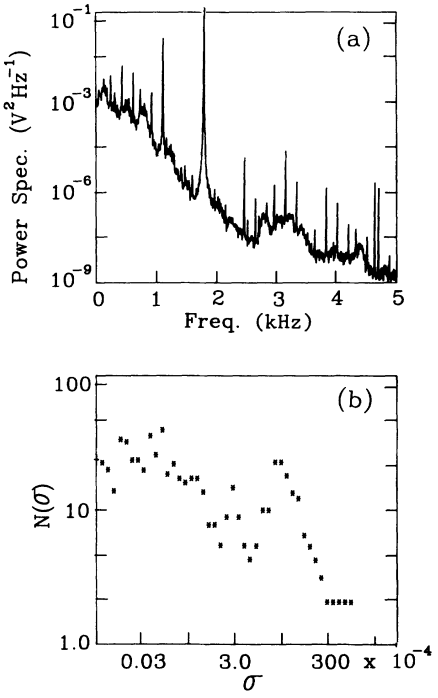

FIG. 6. (a) A power spectrum obtained by analog simulation for the fixed conditions and $q_2=0.38$ (chaotic), and (b) the threshold dependence of the number of peaks.

tions identical to those of the attractors shown in Figs. 3 and 4. The most striking difference is that the multitude of peaks evident in Fig. 5(a) are broadened in Fig. 6(a) with only a few dominant ones remaining. The latter clearly results from a chaotic system, while the former might well be supposed to result from a very complex quasiperiodic attractor. We have attempted to apply the criterion given by Eqs. (1) to these two power spectra, that is, we have counted the number of peaks $N(\sigma)$ with amplitudes greater than a threshold σ. The results, plotted on a log-log scale, are shown below their respective power spectra in Figs. 5(b) and 6(b). While it is not quite possible to match the results shown in Fig. 5(b) to a pure power law as indicated by Eq. 1(a), that seems closer to an appropriate description than that of the results shown in Fig. 6(b). It is possible that the washing out of the very fine structure by the inherent noise in the analog system and/or the smearing of some of the finer peaks in the frequency spectra by phase noise in the synthesizers may have obscured the power-law dependence of $N(\sigma)$ on σ.

We now turn our attention to the information dimension, defined in the usual way [6,20]:

$$D_I = \lim_{e \to 0} \left[\frac{I(e)}{\log_{10}(1/e)} \right] , \tag{5}$$

where e is the box size in phase space and $I(e)$ is the information

$$I(e) = - \sum_{i=1}^{N(e)} P_i \ln P_i , \tag{6}$$

with P_i the frequency at which box i is visited by the dynamics. We have measured this dimension on data provided by the analog simulator from the reduced, two-dimensional (Poincaré) section. In Fig. 7(a) we have plotted $I(e)$ versus $\log_{10}(1/e)$ for the two attractors shown in Figs. 3 and 4. Over the range in e above a lower limit set by the inherent noise, we find a good linear behavior of $I(e)$ on $\log_{10}(1/e)$ as shown by the straight lines, the slopes of which give D_I. We find that $D_I \cong 1.19$ for the attractor of Fig. 3 to be contrasted with $D_I \cong 1.58$ for the attractor of Fig. 4. The former result is in good agreement with both the predictions and the numerical results of Ding, Grebogi, and Ott [6] for a SNCA. Since the measurement of dimension on real physical systems, which are always to some degree contaminated by noise, is often open to criticism, we have tested our algorithm on measured sets of data of various sizes for the SNCA of Fig. 3. These results are shown in Fig. 7(b), where it is evident that data sets varying in size from 10^4 to 10^5 points yield substantially the same fitted slope if rounding at the high and low ends of the $\log_{10}(1/e)$ scale is neglected. At the high end there is more rounding for the smaller data sets, as expected.

We consider now the destruction of the chaotic attractor which existed at $q_2 = 0.38$ and its replacement by a SNCA at a critical value $q_{2\text{crit}} \cong 0.612$. These results were obtained by digital simulation, and the only criterion used to determine the type of dynamics was the Lyapunov exponent. By measuring λ for each attractor obtained from stepping q_2 between the two limits given

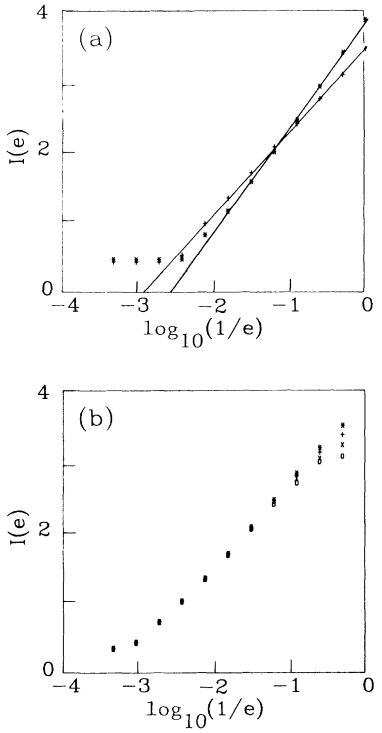

FIG. 7. The information vs the logarithm of the reciprocal box size obtained from analog measurements: (a) The crosses are for $q_2 = 0.88$ (SNCA) and the asterisks are for $q_2 = 0.38$ (chaotic). The straight lines have slopes $D_I \cong 1.19$ (+) and $D_I \cong 1.58$(*). The size of the data sets was 10^5 points. (b) A test of the dependence of D_I on the data-set size from analog measurements: (○) 10^4, (×) 2×10^4, (+) 4×10^4, and (*) 10^5 points, respectively. The logarithms are base 10.

above, we determined the value of $q_{2\text{crit}}$ at which λ passed through zero. Treating $|\lambda|$ as an order parameter, we then made the plot shown in Fig. 8. Least-squares fits to obtain the straight lines shown indicate that the results

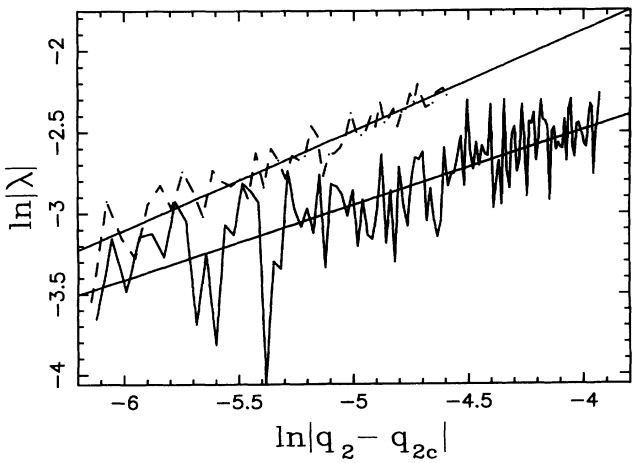

FIG. 8. The Lyapunov exponent as an order parameter in the destruction of chaos by a SNCA. The results for the chaotic attractor are shown by the dash-dotted line, and for the SNCA by the solid line. The straight lines are least-squares fits to the data and have slopes 0.613 and 0.463 for the chaotic and nonchaotic attractors, respectively.

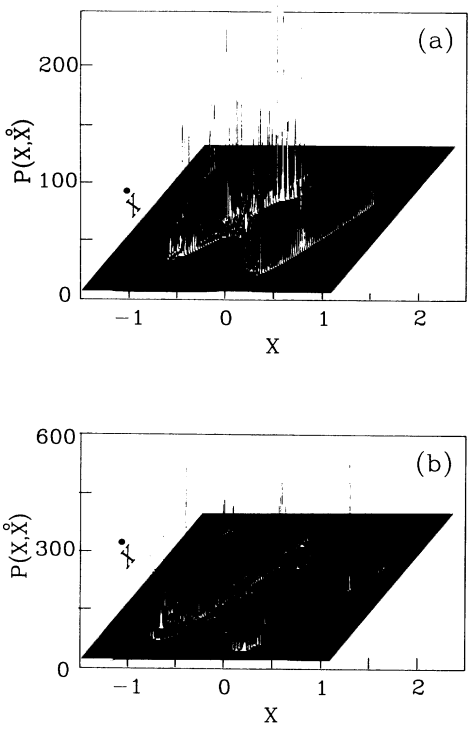

FIG. 9. The invariant densities for the attractors shown in Figs. 3 and 4, measured on the analog simulator using data sets of 10^5 points each: (a) for the chaotic attractor with the fixed conditions and $q_2=0.38$, and (b) for the SNCA with fixed conditions and $q_2=0.88$. The velocity $\dot{x}$ is plotted on the isometric axis vs the coordinate x on the horizontal axis.

behave according to a power law,

$$|\lambda|^{\alpha} \propto |q_2 - q_{2\text{crit}}| \ , \tag{7}$$

with $\alpha \cong 0.463$ for the SNCA and $\alpha \cong 0.613$ for the chaotic attractor. We note also the much greater variability of λ for the SNCA, an effect, noted in Ref. [7], which possibly contributes to the difficulty encountered in attempts to measure it experimentally from Poincaré sections.

Finally, we present also without analysis another measure, the invariant density, which shows differences between the two attractors shown in Figs. 3 and 4. We measured the two-dimensional densities $P(\dot{x},x)$ using the analog simulator, with the results shown in Fig. 9(a) for the chaotic attractor and 9(b) for the SNCA. We note that $P(\dot{x},x)$ is much more sharply defined for the SNCA than for the chaotic attractor. This is indicated by the amplitudes of the peaks, both densities having been obtained from the same number of digitized points (10^5). The chaotic attractor displays a considerably smaller amplitude and shows less fine detail as expected from a higher-dimensional object. It may be possible to develop an additional criterion based on the differences in these densities.

IV. SUMMARY AND CONCLUDING REMARKS

We have demonstrated, with measurements on an analog simulator—a real physical system—for a particular multistable potential not previously studied, that the dynamics [1–6] observed in bistable magnetic beam experiments [7,8] is robust to the small inherent noise encountered in experimental systems, exists over a region of parameter space of nonzero measure, and is easily observable using criteria based on the Lyapunov exponent, information dimension, and characteristics of the power spectra. Moreover, we have shown that a SNCA can destroy and replace a chaotic attractor. We have displayed this phenomenon as a classical phase transition using the Lyapunov exponent as an order parameter, whereupon we obtained substantially different power-law exponents for the SNCA compared to the chaotic attractor. Finally, we suggest that our simulations can be viewed as a prelude to further experimentation on SNCA's with irrationally forced r.f SQUID's, whose potential, with regard to the magnetic flux internal to the SQUID loop, is similar to the one used here.

ACKNOWLEDGMENTS

We are grateful to Edward Ott and Mingzhou Ding who originally encouraged us to search for SNCA's with an analog simulation. Thanks are due also to William Ditto for many stimulating discussions. This work was supported by the Office of Naval Research Grant Nos. N00014-90-J-1327 and N00014-90-AF-001.

[1] C. Grebogi, E. Ott, S. Pelikan, and J. A. Yorke, Physica **13D**, 261 (1984).
[2] A. Bondeson, E. Ott, and T. Antonsen, Phys. Rev. Lett. **55**, 2103 (1985).
[3] F. Romeiras, A. Bondeson, E. Ott, T. Antonsen, and C. Grebogi, Physica **26D**, 277 (1987).
[4] F. Romeiras and E. Ott, Phys. Rev. A **35**, 4404 (1987).
[5] M. Ding, C. Grebogi, and E. Ott, Phys. Rev. A **39**, 2593 (1989).
[6] M. Ding, C. Grebogi, and E. Ott, Phys. Lett. A **137**, 167 (1989).
[7] W. Ditto, M. Spano, H. Savage, S. Rauseo, J. Heagy, and E. Ott, Phys. Rev. Lett. **65**, 533 (1990).
[8] J. Heagy and W. Ditto, J. Nonlin. Sci. **1**, 423 (1991).
[9] J. Kaplan and J. A. Yorke, *Functional Differential Equations and the Approximation of Fixed Points* (Springer-Verlag, Berlin, 1978), p. 288.
[10] T. Kapitaniak, E. Ponce, and J. Wojewoda, J. Phys. A **23**, L383 (1990).
[11] T. Kapitaniak and J. Wojewoda, J. Sound Vib. **138**, 162 (1990).
[12] T. Kapitaniak and M. S. El Naschie, Phys. Lett. A **154**, 249 (1991).
[13] S. Wiggins, Phys. Lett. A **124**, 138 (1987).
[14] F. C. Moon and W. T. Holmes, Phys. Lett. **111A**, 157 (1985).
[15] P. V. E. McClintock and F. Moss, in *Noise in Nonlinear Dynamical Systems,* edited by F. Moss and P. V. E.

McClintock (Cambridge University Press, Cambridge, 1989), Vol. 3, p. 243.

[16] *Computing Before Computers,* edited by W. Aspray (Iowa State University Press, Ames, 1990).

[17] J. Smythe, F. Moss, and P. V. E. McClintock, Phys. Rev. Lett. **51**, 1062 (1983); L. Gammaitoni, F. Marchesoni, E. Menichella-Saetta, and S. Santucci, *ibid.* **62**, 349 (1989); T. Zhou and F. Moss, Phys. Rev. A **41**, 4255 (1990).

[18] I. Shimada and T. Nagashima, Prog. Theor. Phys. **61**, 1605 (1979); G. Benettin, L. Galgani, A. Giorgilli, and J. Streleyn, C. R. Acad. Sci. Paris **286**, A-431 (1978).

[19] A. Wolf, J. Swift, H. L. Swinney, and J. A. Vastano, Physica D **16**, 285 (1985).

[20] See, for example, T. S. Parker and L. O. Chua, *Practical Numerical Algorithms for Chaotic Systems* (Springer-Verlag, Berlin, 1989), Chap. 7.

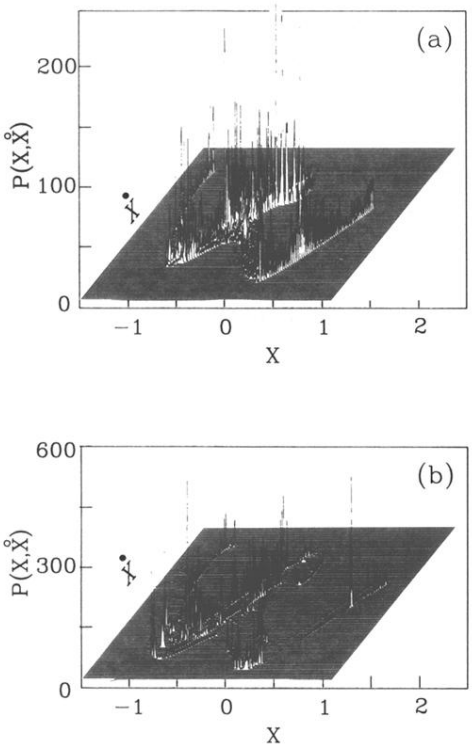

FIG. 9. The invariant densities for the attractors shown in Figs. 3 and 4, measured on the analog simulator using data sets of 10^5 points each: (a) for the chaotic attractor with the fixed conditions and $q_2=0.38$, and (b) for the SNCA with fixed conditions and $q_2=0.88$. The velocity $\dot{x}$ is plotted on the isometric axis vs the coordinate x on the horizontal axis.